Structural changes during HCN channel gating defined by high affinity metal bridges

Daniel C.H. Kwan,[1] David L. Prole,[1,2] and Gary Yellen[1]

[1]Department of Neurobiology, Harvard Medical School, Boston, MA 02115
[2]Department of Pharmacology, University of Cambridge, Cambridge CB2 1PD, England, UK

Hyperpolarization-activated cyclic nucleotide–sensitive nonselective cation (HCN) channels are activated by membrane hyperpolarization, in contrast to the vast majority of other voltage-gated channels that are activated by depolarization. The structural basis for this unique characteristic of HCN channels is unknown. Interactions between the S4–S5 linker and post-S6/C-linker region have been implicated previously in the gating mechanism of HCN channels. We therefore introduced pairs of cysteines into these regions within the sea urchin HCN channel and performed a Cd^{2+}-bridging scan to resolve their spatial relationship. We show that high affinity metal bridges between the S4–S5 linker and post-S6/C-linker region can induce either a lock-open or lock-closed phenotype, depending on the position of the bridged cysteine pair. This suggests that interactions between these regions can occur in both the open and closed states, and that these regions move relative to each other during gating. Concatenated constructs reveal that interactions of the S4–S5 linker and post-S6/C-linker can occur between neighboring subunits. A structural model based on these interactions suggests a mechanism for HCN channel gating. We propose that during voltage-dependent activation the voltage sensors, together with the S4–S5 linkers, drive movement of the lower ends of the S5 helices around the central axis of the channel. This facilitates a movement of the pore-lining S6 helices, which results in opening of the channel. This mechanism may underlie the unique voltage dependence of HCN channel gating.

The Journal of General Physiology

INTRODUCTION

Hyperpolarization-activated cyclic nucleotide–sensitive nonselective cation (HCN) channels are members of the pore-loop cation channel superfamily, which includes voltage-gated potassium (Kv) channels (Gauss et al., 1998; Ludwig et al., 1998; Yu et al., 2005). However, unlike Kv channels and most other voltage-gated cation channels that open with membrane depolarization, HCN channels activate in response to membrane hyperpolarization. HCN channels underlie the funny current in the heart (Ludwig et al., 1998) and the hyperpolarization-activated current in neurons (Santoro et al., 1998). These hyperpolarization-activated inward currents serve as the initial depolarizing current for firing an action potential in excitable cells, thus allowing cardiac myocytes and neurons to generate rhythmic firing behavior (Hille, 2001).

HCN channels share common structural features with both Kv channels and CNG channels (Craven and Zagotta, 2006). Each HCN channel is thought to consist of four subunits arranged with fourfold symmetry, with each subunit containing six transmembrane segments (S1–S6) as well as intracellular N and C termini (Fig. 1 A). Like Kv channels, HCN channels have a voltage-sensing domain (VSD) comprised of the first four transmembrane segments (S1–S4), with the S4 voltage sensor bearing positively charged residues. The S4–S5 linker joins the VSD to the pore domain, which includes S5, S6, and the P-loop. The activation gate is formed by the lower S6 (Shin et al., 2001; Rothberg et al., 2002), which in turn is joined to the C-terminal cyclic nucleotide–binding domain (CNBD) via the C-linker (Fig. 1 A). Similar to its function in CNG channels, the CNBD in HCN channels binds cAMP directly to confer cyclic nucleotide sensitivity and promote channel opening (Zagotta et al., 2003). Despite sharing structural similarities with Kv and CNG channels, HCN channels show distinct biophysical properties that make them unique among voltage-gated ion channels. Foremost among these is their activation by hyperpolarized membrane potentials. Based on accessibility experiments, the VSD of HCN channels has been shown to function similarly to that of Kv channels, with inward movement of S4 occurring in response to hyperpolarization (Männikkö et al., 2002). HCN and Kv channels also both possess intracellular gates within their lower S6 segments (Liu et al., 1997; Shin et al., 2001; Rothberg et al., 2002). Thus, both the

D.C.H. Kwan and D.L. Prole contributed equally to this paper.
Correspondence to Gary Yellen: gary_yellen@hms.harvard.edu

Abbreviations used in this paper: CNBD, C-terminal cyclic nucleotide–binding domain; HCN, hyperpolarization-activated cyclic nucleotide–sensitive nonselective cation; Kv, voltage-gated potassium; spHCN, sea urchin HCN; VSD, voltage-sensing domain; WT, wild type.

The Rockefeller University Press $30.00
J. Gen. Physiol. Vol. 140 No. 3 279–291
www.jgp.org/cgi/doi/10.1085/jgp.201210838

voltage sensor and gate are similar to those of Kv channels, and it is likely the details of the coupling between the two that determines the reversed voltage dependence of HCN channels.

Electromechanical coupling in voltage-gated ion channels has been proposed to involve the S4–S5 linker and the lower S6 (Chen et al., 2001; Bell et al., 2009). However, the detailed interactions between these two regions have not yet been fully resolved. Some understanding of this process in Kv channels has been gained from the crystal structures of Kv1.2 and a related Kv channel chimera (Long et al., 2005a,b, 2007). In the presumed open state of Kv1.2, the S4–S5 linker of one subunit rests on top of the lower S6 of the same subunit, where "top" indicates toward the extracellular side when the channel is viewed from the membrane. It has been proposed that a downward motion of the S4 and the S4–S5 linker pushes the S6 downward, restricting the opening formed by the four S6 bundles and hence closing the activation gate (Long et al., 2005b). Compatibility is required between the S4 voltage sensor and the S6 activation gate to confer voltage-sensitive gating in Kv channels (Lu et al., 2002). This suggests that some specificity is present in the interaction between the S4–S5 linker and the S6. For HCN channels, an involvement of interactions between the S4–S5 linker and the post-S6 in electromechanical coupling has also been shown. For example, in the closed state an arginine residue located at the distal end of the S4–S5 linker has been proposed to interact with an aspartate residue in the proximal C-linker (Decher et al., 2004). In addition, cross-linking the S4–S5 linker and C-linker reverses the apparent voltage dependence of sea urchin HCN (spHCN) channels (Prole and Yellen, 2006). Interactions between the S4–S5 linker and post-S6 may therefore contribute to the unique voltage sensitivity of HCN channels. Hence, we set out to define the spatial relationship between the S4–S5 linker and post-S6/C-linker in HCN channels using high affinity metal bridges.

We performed a Cd^{2+} scan in spHCN channels, with cysteine mutations introduced into both the S4–S5 linker and the lower S6/C-linker region (Fig. 1 B), either singly or in pairs. When Cd^{2+} is applied to the cytoplasmic side of the channel, a pair of cysteine residues with a favorable separation distance and geometry can be bridged by a Cd^{2+} ion, thus locking the channel in a particular state, as shown in previous studies (Yellen et al., 1994; Holmgren et al., 1998; Rothberg et al., 2002). By using different pairs of residues, we were able to map the interactions between the S4–S5 linker and the lower S6/C-linker in both the open and closed conformations. We found that bridging pairs of cysteines in the S4–S5 linker and the lower S6/C-linker with Cd^{2+} traps the spHCN channel in either the open or closed state, depending on the locations of the cysteine pairs. This suggests that the S4–S5 linker and post-S6/C-linker can interact in both the open and closed states. We then used dimeric concatemers of spHCN channel subunits to define the location of coordination sites within the context of the tetrameric channel. Significantly, we found that the S4–S5 linker is in close proximity to the post-S6/C-linker of a neighboring subunit in both the open and closed states. The observed proximities of the S4–S5 and post-S6/C-linker regions cannot be mapped consistently to models based on the crystal structures of depolarization-activated Kv1.2 channels (Long et al., 2005b) or a Kv1.2/Kv2.1 chimera (Long et al., 2007). A structural model of the spHCN channel based on our data suggests significant differences from the structures and gating motions of depolarization-activated channels, which may underlie the unique voltage dependence of HCN channels.

MATERIALS AND METHODS

Molecular biology and expression of spHCN channels

Mutants of the spHCN1 channel subunit (available from GenBank/EMBL/DDBJ under accession no. Y16880) were generated as described previously (Shin et al., 2001). In brief, site-directed mutagenesis was performed with appropriate PCR primers and the product subcloned back into the parental vector (pcDNA4.1; Invitrogen). All subunits contained the M349I and H462Y mutations as described previously (Rothberg et al., 2003). Additionally, C211Y, C224I, C254V, and C266M mutations in the N terminus as well as C369F and C373G in the lower S5 were introduced to form a partially cysteineless background, which we termed the "wild-type" (WT) channel. Tandem dimer constructs were generated as described previously (Rothberg et al., 2002). In brief, the stop codon from the "A" protomer was replaced by a linker into which the "B" protomer was inserted. All mutations and tandem dimers were confirmed by sequencing.

Human embryonic kidney (HEK-293) cells were maintained under a 5% CO_2 atmosphere at 37°C in MEM supplemented with 10% FBS. Cells were used from 1 wk after thawing for ~30 subsequent passages. Trypsinized HEK-293 cells suspended in cold HEPES-buffered saline were mixed with cDNA for spHCN channels (20–30 µg) and the πH3-CD8 plasmid (1 µg), transfected using electroporation, and plated on protamine-coated coverslips 1–2 d before experiments. Binding of anti-CD8 antibody–coated Dynabeads (1 µl applied to each coverslip of cells for 15 min immediately before recording; Invitrogen) was used to identify transfected cells.

Solutions and electrophysiological experiments

HEK-293 cells expressing spHCN channels were pretreated with 5 mM dithiothreitol (DTT) for 15–20 min at 37°C. DTT was then washed off with bath solution (see below) before experiments, which were performed with excised inside-out patches at room temperature (22–25°C), as described previously (Prole and Yellen, 2006). Currents were low-pass filtered at 2–5 kHz and digitized at 10 kHz without leak subtraction. Methods for rapid perfusion switches were as described previously (Liu et al., 1997). Thick-walled borosilicate glass capillaries (Dagan) were pulled to ~1-µm tip diameter and fire-polished before being filled with pipette solution, which contained (in mM): 160 KCl, 10 HEPES, and 0.5 $MgCl_2$, adjusted to pH 7.4 with KOH. The control bath solution contained (in mM): 160 KCl, 10 HEPES, 0.5 $MgCl_2$, 0.2 EGTA, and 0.1 cAMP, adjusted to pH 7.4 with KOH. Bath solution containing

1 µM Cd^{2+} was prepared by adding an appropriate amount of 10 mM $CdCl_2$ stock to a bath solution containing no EGTA. A concentration of 1 µM total Cd^{2+} is equivalent to ~130 nM of free Cd^{2+} in solution (Rothberg et al., 2003). The HCN channel blocker ZD7288 (Tocris) was applied (100 µM in control bath solution) at the end of the experiment to distinguish between HCN current and endogenous background current. DTT was made as a 1-M stock solution in distilled water and applied at the required concentration within 6 h. All chemicals were obtained from Sigma-Aldrich except where noted.

Data analysis

To measure the G-V curves, currents were elicited by 500-ms voltage pulses from a holding potential of 0 mV to potentials ranging from −120 to +50 mV in +10-mV increments, followed by 500-ms voltage pulses at +50 mV to record the tail currents. Currents recorded at 5 ms after the start of the tail were plotted against the voltage of the test pulse and fit to a modified Boltzmann function ($y = (y_{max} - y_0)/exp(-(V - V_{1/2})/k) + y_0$), where y_{max} is the maximum tail current, y_0 is the minimum current, V is the voltage of the test pulse, $V_{1/2}$ is the half-activation voltage, and k is the slope factor. The currents were then normalized to ($y_{max} - y_0$) and fit to the above equation with $y_0 = 0$ and $y_{max} = 1$. The final fitted parameters were then averaged over n experiments.

To quantify the extent of lock-open effects, the nondecaying portion of tail currents recorded at +50 mV was measured by fitting the tail currents to a double-exponential function. The extent of lock-open was given as the proportion of the constant term relative to the total current magnitude in the fit. Cd^{2+} was considered to lock open a double mutant if this quantified extent of lock-open was increased by Cd^{2+} and was significantly larger than in both the single mutant controls.

For assessing lock-closed effects, we compared the 10–50% rise time ($RT_{10-50\%}$) during a hyperpolarizing pulse in the presence of Cd^{2+} to that without Cd^{2+}. The time-dependent portion of test currents observed at −120 mV was fit to either a single- or double-exponential function, and the maximum current within the first 500 ms was determined for calculating the time elapsed between reaching 10 and 50% of that maximum current. Cd^{2+} was considered to lock closed a double mutant if the quantified extent of the lock-closed effect was increased by Cd^{2+} and was significantly larger than in both the single mutant controls. All experimental values are expressed as mean ± SEM. Statistical significance was assessed using an unpaired t test, and values were judged to be significantly different if $P < 0.05$.

RESULTS

To identify state-dependent interactions between the S4–S5 linker and post-S6/C-linker in spHCN channels, paired cysteine mutations were introduced into these regions (Fig. 1 B), and the effect of Cd^{2+} on the gating of these mutants was assessed in the constant presence of saturating cAMP. We refer to stabilization of the open and closed states by Cd^{2+} as lock-open and lock-closed effects, respectively. All mutants were made on a partially cysteineless background, which we term WT, to minimize background reactivity. WT channels gate normally and exhibit no significant response to Cd^{2+} (Fig. 2).

We first tested single cysteine mutants in the post-S6/C-linker region. Among the mutants tested, D471C, R475C, Y477C, and K480C did not show appreciable current (not depicted), and we did not test these mutants further. In contrast, the other single mutants (S472C, S473C, S474C, Q476C, R478C, E479C, K482C, and E485C) show robust currents (Fig. 2). Although these mutants were made on the partially cysteineless background, all except E485C show some degree of current inhibition by Cd^{2+} (Fig. 2). This current inhibition is relatively small in most instances and may relate to an inactivation process, as suggested in a previous study (Prole and Yellen, 2006). The single mutants show no significant lock-open or lock-closed behavior (Fig. 2), with the exception of S474C, which shows mild lock-open and lock-closed effects. The effects of Cd^{2+} on these mutants are summarized in Table 1. Using these single mutants as controls, we tested which pairs of introduced cysteine residues could form stable metal bridges with Cd^{2+} in either the open or the closed state.

Metal bridges define the state-dependent proximity of S4–S5 linker and C-linker regions

The S4–S5 linker single mutants F359C, V361C, and A364C show only relatively small effects of Cd^{2+} (Figs. 2

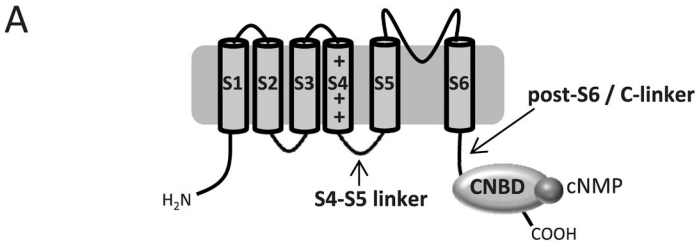

B

```
                 S4                  S4-S5 linker
spHCN1:  RALKILRFAKLLSLLRLLRLSRLMRFVSQWEQAFN----VANAVIR 367
hCN2 :   RALRIVRFTKILSLLRLLRLSRLIRYIHQWEEIFHMTYDLASAVMR 366
hKv1.2:  MSLAILRVIRLVRVFRIFKLSRHSKGLQILGQTLK-------ASMR 326

                 S6                  post S6 / C-linker
spHCN1:  WLTIVSMVSGATCFALFIGHATNLIQSMDSSSRQYREKLKQVEEYMQYR 491
hCN2 :   WLTMLSMIVGATCYAMFIGHATALIQSLDSSRRQYQEKYKQVEQYMSFH 490
hKv1.2:  IVGSLCAIAGVLTIALPVPVIVSNFNYFYHRETE-GEEQAQYLQVTSCP 436
KcsA  :  LVAVVVMVAGITSFGLVTAALATWFVGREQERRGHFVRHSEKAAEEAYT 138
```

Figure 1. Schematic of the structure of spHCN channel subunits. (A) Schematic of the putative topology of an spHCN subunit. Locations of the charged S4 voltage sensor, the S4–S5 linker, the post-S6/C-linker, the CNBD, and the binding site for cyclic nucleotide monophosphate (cNMP) are shown. (B) Sequence alignments of the S4, S4–S5 linker, pore-lining S6, and post-S6/C-linker regions of spHCN1 (GenBank accession no. CAA76493), with human Kv1.2 (NCBI Protein database accession no. NP_004965), rat Kv1.2 (NCBI Protein database accession no. NP_037102), and KcsA (UniProtKB/Swiss-Prot sequence P0A334) channel subunits. Alignments were made using ClustalW2. Mutations of spHCN1 discussed in Results and Discussion are shown as bold and underlined.

and 3, and Table 1). When F359C was paired with the various C-linker cysteine mutations, all but the double mutant 359C479C produced robust currents (Fig. 2). In response to Cd^{2+}, the double mutants 359C474C and 359C485C show an almost complete lock-open effect that is absent in the single mutants (Fig. 2). Other double mutants such as 359C476C and 359C478C fail to show any lock-open effect. The 361C-containing double mutants 361C473C, 361C474C, and 361C485C show prominent lock-open effects in response to Cd^{2+} (Fig. 3). In contrast, effects of Cd^{2+} on 361C478C and 361C479C are not significantly different from those seen with the single mutants. In response to Cd^{2+}, the double mutant 361C476C, and to a lesser extent 361C472C, shows pronounced slowing of activation kinetics (Fig. 3). This is indicative of a lock-closed effect, reminiscent of that induced by Cd^{2+} in spHCN channels containing a proximal post-S6 cysteine (Q468C) (Rothberg et al., 2003). The most interesting and unambiguous effects of Cd^{2+} occur with the A364C double mutants (Fig. 3). The double mutants 364C482C and 364C485C show pronounced lock-open, whereas 364C472C shows lock-open with substantial current inhibition (Fig. 3). Most dramatically, several A364C-containing double mutants show a prominent lock-closed effect (Fig. 3), including all those with cysteine residues located between positions 473

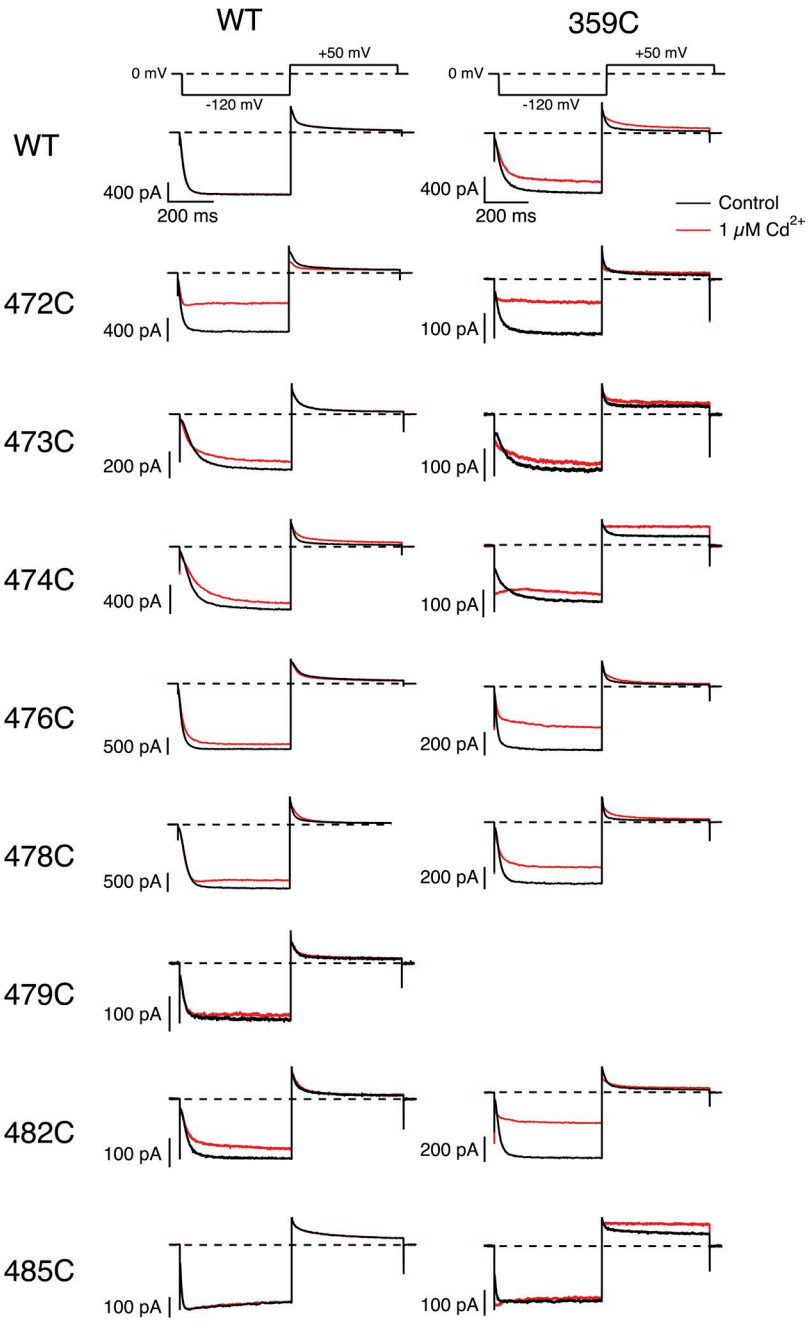

Figure 2. Metal bridges can form between the S4–S5 linker and C-linker in the open state. Representative current traces of selected single C-linker residue mutants and double mutants with F359C. Currents were elicited by 500-ms voltage steps to −120 mV from a holding potential of 0 mV, followed by a voltage step to +50 mV. Currents were recorded in the absence (black) or presence (red) of 1 μM Cd^{2+} from excised inside-out patches expressing the various mutants as indicated. Current traces recorded from the WT partial cysteine-less background, which contains C211Y, C224I, C254V, C266M, C369F, and C373G in addition to the M349I and H462Y mutations, are shown. Current traces recorded from the single F359C mutant are also shown, as well as current traces recorded from single S472C, S473C, S474C, Q476C, R478C, E479C, K482C, and E485C mutants. Current traces from double mutants containing F359C and each of the C-linker mutations are also shown.

TABLE 1

Effects of Cd^{2+} on spHCN channels containing introduced cysteine residues

Construct	Effect	Control					1 μM Cd^{2+}				
		$V_{1/2}$	k	$f_{nondecaying}$	$RT_{10–50\%}$	n	$V_{1/2}$	k	$f_{nondecaying}$	$RT_{10–50\%}$	n
		mV	*mV*		*ms*		*mV*	*mV*		*ms*	
WT		−63 ± 2	6.7 ± 0.3	0.04 ± 0.01	12 ± 1	3	−65 ± 2	6.3 ± 0.1	0.03 ± 0.01	12.5 ± 0.4	3
S472C		−56 ± 5	5.1 ± 0.5	0.03 ± 0.02	8.8 ± 0.6	3	−53 ± 4	4.7 ± 0.7	0.08 ± 0.03	5.3 ± 0.8[a]	3
S473C		−73 ± 2	8.1 ± 0.4	0.09 ± 0.03	23 ± 3	5	−68 ± 2[a]	7.8 ± 0.9	0.13 ± 0.05	23 ± 3	5
S474C		−67 ± 2	6.4 ± 0.1	0.03 ± 0.03	21 ± 5	4	−56 ± 5[a]	10 ± 2[a]	0.24 ± 0.04[a]	58 ± 10[a]	4
Q476C		−56 ± 4	10 ± 2	0.09 ± 0.03	8.3 ± 0.9	4	−62 ± 3	11 ± 3	0.12 ± 0.06	11.2 ± 0.8	4
R478C		−79 ± 1	6.7 ± 0.3	0.08 ± 0.02	20 ± 2	5	−67 ± 1	7.2 ± 0.6	0.08 ± 0.03	20 ± 1	3
E479C		−63 ± 3	12 ± 1	0.05 ± 0.01	12 ± 1	3	−62 ± 3	10 ± 2	0.09 ± 0.03	11 ± 1	3
K482C		−72 ± 4	10 ± 1	0.09 ± 0.03	20 ± 5	4	−69 ± 4	11 ± 2	0.12 ± 0.03	26 ± 6	4
E485C		−50 ± 1	8 ± 1	0.34 ± 0.11	4.8 ± 0.4	3	−49 ± 1	7.4 ± 0.9	0.37 ± 0.12	8 ± 1	3
F359C		−65 ± 3	8.1 ± 0.3	0.07 ± 0.02	15 ± 3	4	−56 ± 2[a]	12 ± 1[a]	0.19 ± 0.01	19 ± 5	4
+S472C		−63 ± 2	10 ± 2	0.12 ± 0.06	16 ± 3	4	−68 ± 7	14 ± 4	0.31 ± 0.07	11 ± 1	4
+S473C	LC	−69 ± 2	8.7 ± 0.7	0.08 ± 0.04	16 ± 2	3	−58 ± 8	14 ± 3	0.12 ± 0.04	56 ± 4[a]	3
+S474C	LO	−57 ± 4	7.2 ± 0.7	0.20 ± 0.08	24 ± 2	3	ND	ND	0.81 ± 0.06[a]	ND	3
+Q476C		−54 ± 5	8 ± 1	0.12 ± 0.01	9 ± 1	3	−54 ± 7	12 ± 3	0.21 ± 0.02	16 ± 4	3
+R478C		−73 ± 3	6.2 ± 0.3	0.04 ± 0.02	14 ± 2	3	−55 ± 2[a]	12.6 ± 0.2[a]	0.17 ± 0.01	20 ± 1[a]	3
+K482C		−61 ± 3	6.3 ± 0.3	0.04 ± 0.01	14 ± 1	3	−36 ± 3[a]	19 ± 3[a]	0.22 ± 0.03[a]	22 ± 3	3
+E485C	LO	−41 ± 5	8.3 ± 0.2	0.31 ± 0.09	4.3 ± 0.2	3	ND	ND	0.84 ± 0.09[a]	ND	3
V361C		−53 ± 3	7.0 ± 0.8	0.20 ± 0.07	8.7 ± 0.8	3	−53 ± 3	12 ± 4	0.36 ± 0.08	10 ± 1	3
+S472C	LC	−59 ± 3	7 ± 2	0.21 ± 0.03	11 ± 1	3	−73 ± 4	10 ± 1	0.19 ± 0.02	25 ± 3[a]	3
+S473C	LO	−77 ± 2	7.7 ± 0.2	0.07 ± 0.03	23 ± 2	3	−55 ± 1[a]	13 ± 1[a]	0.61 ± 0.09[a]	15 ± 2[a]	3
+S474C	LO	−59 ± 4	6.9 ± 0.9	0.22 ± 0.05	12 ± 3	3	ND	ND	0.80 ± 0.01[a]	ND	3
+Q476C	LC	−51 ± 3	4 ± 3	0.15 ± 0.06	6.3 ± 0.2	5	−60 ± 2[a]	8.2 ± 0.4	0.20 ± 0.04	30 ± 6[a]	5
+R478C	LC	−72 ± 2	6.3 ± 0.4	0.02 ± 0.01	9.9 ± 0.8	4	−70 ± 3	8.9 ± 0.8[a]	0.26 ± 0.05[a]	16 ± 2[a]	3
+E479C		−65 ± 4	11 ± 1	0.07 ± 0.02	11 ± 1	4	−68 ± 3	15 ± 5	0.28 ± 0.02[a]	11 ± 1	4
+K482C		−63 ± 3	6.2 ± 0.6	0.13 ± 0.04	10 ± 2	3	−47 ± 3[a]	10.7 ± 0.8[a]	0.42 ± 0.06[a]	10 ± 2	3
+E485C	LO	−41 ± 1	8 ± 2	0.51 ± 0.03	3.5 ± 0.7	3	−84 ± 5[a]	20 ± 3	0.94 ± 0.01[a]	9 ± 2	3
A364C		−53 ± 2	8 ± 1	0.08 ± 0.01	8.2 ± 0.4	3	−56 ± 3	7.9 ± 0.9	0.12 ± 0.03	9.6 ± 0.4	3
+S472C	LO	−47 ± 2	8 ± 1	0.22 ± 0.03	15 ± 3	3	−68 ± 1[a]	20 ± 7	0.66 ± 0.01[a]	33 ± 7	3
+S473C	LC	−69 ± 5	7.9 ± 0.7	0.17 ± 0.04	15 ± 3	3	−89 ± 3[a]	8.6 ± 0.8	0.08 ± 0.04	94 ± 13[a]	3
+S474C	LC	−54 ± 8	8.4 ± 0.2	0.19 ± 0.01	10 ± 3	3	−93 ± 6[a]	7.6 ± 0.3	0.03 ± 0.02[a]	150 ± 10[a]	3
+Q476C	LC	−49 ± 3	8.0 ± 0.3	0.14 ± 0.01	7.6 ± 0.5	3	−98 ± 1[a]	9.4 ± 0.8	0.08 ± 0.01[a]	163 ± 1[a]	3
+R478C	LC	−73 ± 2	6.8 ± 0.2	0.06 ± 0.01	13 ± 2	3	−101 ± 2[a]	6.0 ± 0.8	0.03 ± 0.02	127 ± 5[a]	3
+E479C	LC	−61 ± 3	15 ± 2	0.15 ± 0.03	16 ± 2	5	−75 ± 4[a]	22 ± 4	0.20 ± 0.04	40 ± 7[a]	5
+K482C	LO	−54 ± 2	8 ± 1	0.14 ± 0.01	12 ± 2	4	ND	ND	0.89 ± 0.02[a]	ND	4
+E485C	LO	−32 ± 5	8 ± 1	0.28 ± 0.04	5.5 ± 0.8	4	−32 ± 1	5.6 ± 0.4	0.89 ± 0.01[a]	7 ± 1	4
Dimers											
6472_6472	LO	−46 ± 1	5.9 ± 0.2	0.11 ± 0.01	ND	4	−69 ± 4[a]	21 ± 4[a]	0.74 ± 0.01[a]	ND	4
WT_6472	LO	−63 ± 1	6.6 ± 0.6	0.15 ± 0.02	ND	6	−60 ± 2	8.0 ± 0.7[a]	0.27 ± 0.03[a]	ND	6
364C_472C		−63 ± 3	7.2 ± 0.3	0.08 ± 0.02	ND	4	−63 ± 2	8.5 ± 0.4[a]	0.12 ± 0.02	ND	4
6476_6476	LC	−61 ± 1	10 ± 2	ND	10 ± 2	3	−108 ± 7[a]	8 ± 1	ND	195 ± 13[a]	3
WT_6476	LC	−64 ± 1	9 ± 2	ND	10 ± 2	3	−69 ± 2	9.4 ± 0.9	ND	27 ± 5[a]	3
364C_476C	LC	−58 ± 2	8.5 ± 0.7	ND	8.9 ± 0.6	4	−76 ± 1[a]	11 ± 1[a]	ND	40 ± 2[a]	4
6482_6482	LO	−55 ± 3	7 ± 1	0.10 ± 0.01	ND	3	ND	ND	1.0 ± 0.01[a]	ND	3
WT_6482	LO	−65 ± 2	8.2 ± 0.5	0.06 ± 0.02	ND	6	−63 ± 3	11 ± 2	0.25 ± 0.03[a]	ND	6
364C_482C	LO	−67 ± 1	10 ± 1	0.12 ± 0.01	ND	5	−63 ± 2[a]	19 ± 3[a]	0.39 ± 0.04[a]	ND	5

Standard G-V curve parameters, proportions of the nondecaying tail current ($f_{nondecaying}$), and the rise times between 10 and 50% ($RT_{10–50\%}$) of all the constructs tested in this study. G-V curves were constructed from the start of the tail currents at +50 mV after 500-ms hyperpolarizing pulses ranging from −120 to +50 mV and fit to a Boltzmann function for the half-activation voltage ($V_{1/2}$) and slope factor (k) (see Materials and methods). Proportion of the nondecaying tail current ($f_{nondecaying}$) was measured by fitting the tail current to a double-exponential function and extracting the fraction of the constant term. $RT_{10–50\%}$ was measured from fits of the current trace to either a single- or double-exponential function within the 500 ms of the hyperpolarizing pulse to −120 mV. All values are expressed as mean ± SEM. Parameters that have not been determined are indicated as ND. Values for double mutants in the presence of Cd^{2+}, which are significantly different from the corresponding values for both the respective single S4–S5 and C-linker mutants, are shown in bold and underlined. The double mutants that we consider to form lock-open or lock-closed bridges in the presence of Cd^{2+} are indicated.
[a]Significant difference from the value in the absence of Cd^{2+} (unpaired t test; $P < 0.05$).

and 479. The lock-closed effect is strongest in the 364C476C mutant and diminishes for residues located further away from this position within the C-linker. An arginine residue in the S4–S5 linker of HCN2 (R339; corresponding to R367 in spHCN) has been proposed previously to interact with an aspartate residue in the post-S6 (D443; corresponding to D471 in spHCN) when the channel is closed (Decher et al., 2004). However, both the single R367C and D471C mutants failed to express in our hands, and we did not pursue these mutants further.

The lock-open and lock-closed effects for all the mutants tested are summarized in Fig. 4 and Table 1. Although relatively modest, the effects of Cd^{2+} on some single mutants suggested that other endogenous residues might in some cases contribute to coordination of Cd^{2+}, and that a cautious evaluation of lock-open and lock-closed effects was required. We therefore considered lock-open or lock-closed effects to occur only if Cd^{2+} had effects that were significantly larger than in both the respective single mutant controls (Table 1).

Collectively, these results initially allow several conclusions to be drawn. First, the S4–S5 linker and C-linker are in close proximity and can interact in both the open and closed states. Second, in the open state the S4–S5 linker is apparently in close proximity to two different regions of the lower S6/C-linker, centered on the residues at positions 472/474 and 485. Third, in the closed state the C-linker appears to form metal bridges more readily with the distal part of the S4–S5 linker than with the proximal portion, with the S4–S5 linker residue at position 364 in close proximity to the C-linker residue at position 476.

Intersubunit contacts between the S4–S5 linker and C-linker regions

The pattern of lock-open and lock-closed effects for the double mutants involving A364C in the S4–S5

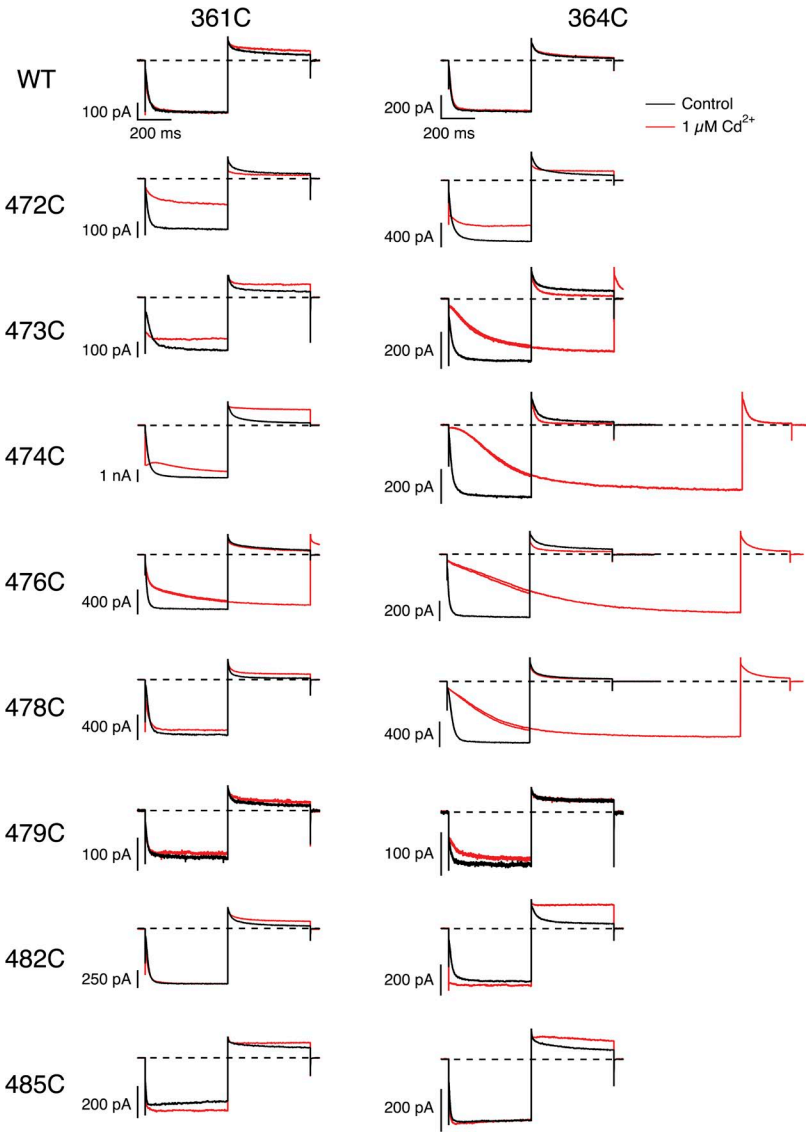

Figure 3. Metal bridges can form between the S4–S5 linker and C-linker in both open and closed states. Representative current traces of selected C-linker mutants with V361C and A364C. Currents were elicited by voltage steps to −120 mV from a holding potential of 0 mV, followed by a voltage step to +50 mV. Currents were recorded in the absence (black) or presence (red) of 1 μM Cd^{2+} from excised inside-out patches expressing the various mutants as indicated. For the V361CQ476C and A364CS473C mutants, currents recorded in response to a 1-s hyperpolarizing pulse from 0 to −120 mV are also shown to highlight the slowing of activation by Cd^{2+}. For the A364CS474C, A364CQ476C, and A364CR478C mutants, currents recorded in response to a 2-s hyperpolarizing pulse from 0 to −120 mV are also shown to highlight the slowing of activation by Cd^{2+}.

linker shows that in the closed state, the residue at position 364 is in close proximity to the C-linker residues at or near position 476. When the channel opens, residue 364 moves close to residues at both positions 472 and 482. Based on the available crystal structure of the CNBD, this region of the C-linker between 472 and 482 is an α-helical structure (Zagotta et al., 2003) that would separate these two residues by ∼15 Å. Therefore, the simplest interpretation of our results is that in the open state, the residue at position 364 can interact with position 472 in one subunit and position 482 on a different subunit.

To test this hypothesis, tandem dimers were constructed by concatenating two spHCN subunits. This allows different types of subunit interactions to be distinguished (Holmgren et al., 1998; Rothberg et al., 2003). We focused mainly on the A364C series, as these mutants show the clearest trend in lock-open and lock-closed profiles. The subunit specificity of the interaction between A364C and S472C was tested with three different tandem constructs. We linked together two 364C472C double mutants (364C472C_364C472C) to control for the effect of the tandem construction; a WT subunit with a 364C472C mutant (WT_364C472C); and an A364C single mutant with a S472C single mutant (364C_472C) to test for an intersubunit interaction, as this latter construct is capable of forming only intersubunit metal bridges between the introduced cysteines. The last two constructs are expected to exhibit smaller Cd^{2+} effects than the control, as they are capable of forming only half the number of possible metal bridges between introduced cysteines. Fig. 5 A shows representative current traces from these three constructs in the absence (black) or presence (red) of Cd^{2+}. As with the "monomeric" 364C472C mutant, the "dimeric" 364C472C mutant (364C472C_364C472C) shows prominent lock-open with Cd^{2+} (Fig. 5 A). The WT_364C472C dimer shows a slight lock-open effect, whereas the intersubunit interacting pair (364C_472C) shows no measurable lock-open effect (Fig. 5, A and B, and Table 1).

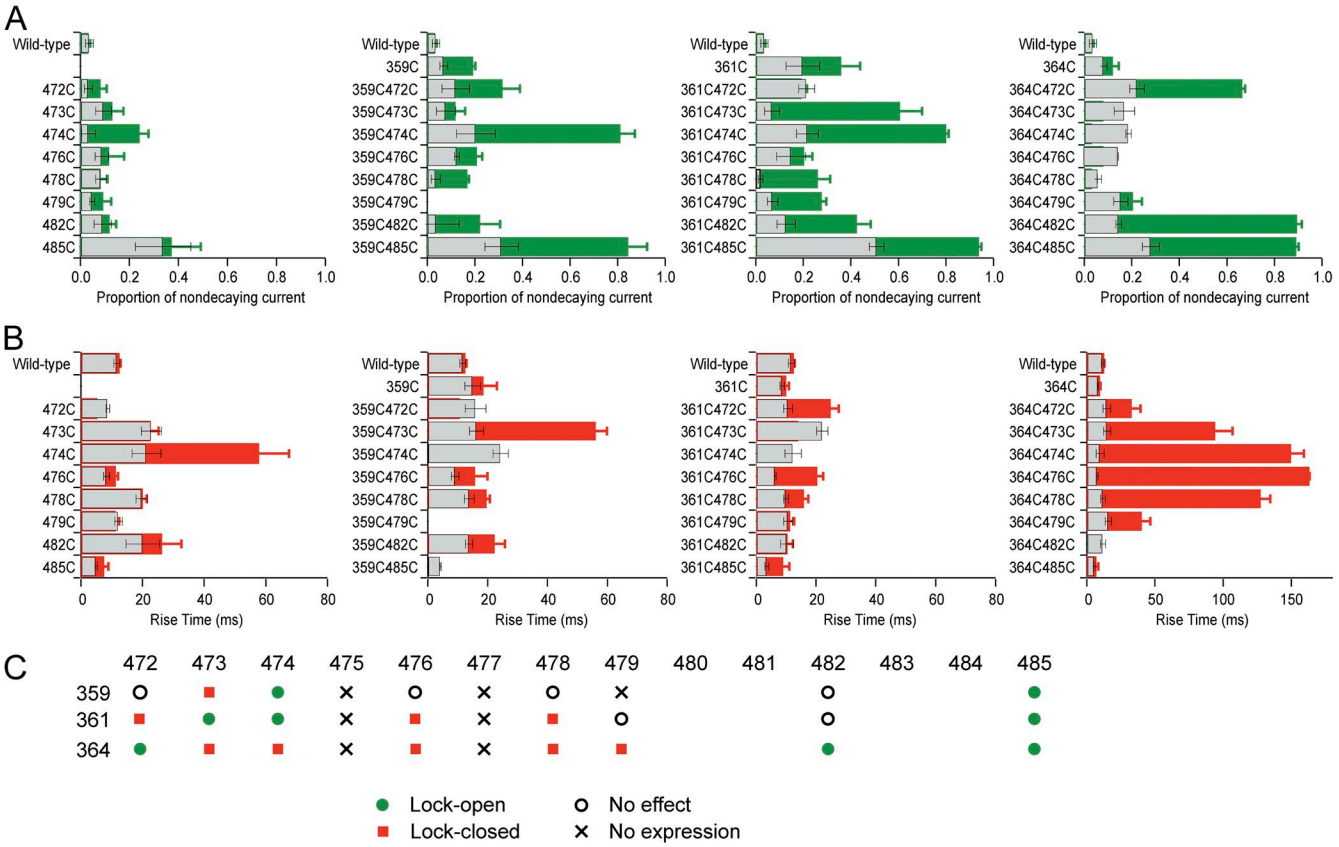

Figure 4. Summary of the effects of Cd^{2+} on spHCN channels containing introduced cysteine residues. (A) The lock-open effects of 1 μM Cd^{2+}, as indicated by the proportion of the nondecaying tail current, in the single C-linker controls (left-most panel) and the double mutants containing one of the F359C, V361C, or A364C mutations are shown. Gray bars indicate values for control conditions, and green bars indicate values after the addition of Cd^{2+}. The mutants giving rise to significant lock-open effects are clustered in two separate regions. (B) The lock-closed effects of 1 μM Cd^{2+}, as indicated by the prolongation of the rise time between 10 and 50% of the maximum current in a 500-ms pulse, in the single C-linker controls (left-most panel) and the double mutants containing F359C, V361C, or A364C mutations are shown. Gray bars indicate values for control conditions, and red bars indicate values after the addition of Cd^{2+}. (C) A summary of the effects of 1 μM Cd^{2+} on the double mutants tested in this study.

These results suggest that in the open state of dimeric constructs, 364C can interact with 472C, possibly within the same subunit, although intersubunit interactions between opposite subunits cannot be excluded.

A lock-open effect caused by Cd^{2+} is also seen for the 364C482C_364C482C dimer (Fig. 6 A), and this effect is retained in the intersubunit 364C_482C dimer, which shows a lock-open effect greater than that of the WT_364C482C dimer (Fig. 6, A and B). This suggests the possibility that 364C and 482C from different subunits may be in close proximity in the open state.

Also informative are the effects of Cd^{2+} on dimers containing A364C together with Q476C (Fig. 7). The 364C476C_364C476C dimer shows dramatic lock-closed effects of Cd^{2+} (Fig. 7 A). This effect is retained in the intersubunit 364C_476C dimer, which exhibits a lock-closed effect that is even more pronounced than for the WT_364C476C dimer (Fig. 7, A–C). Collectively, these results suggest that the S4–S5 linker and the lower S6/C-linker from different subunits may be in close proximity in both open and closed states of HCN channels, as intrasubunit metal bridges cannot form between

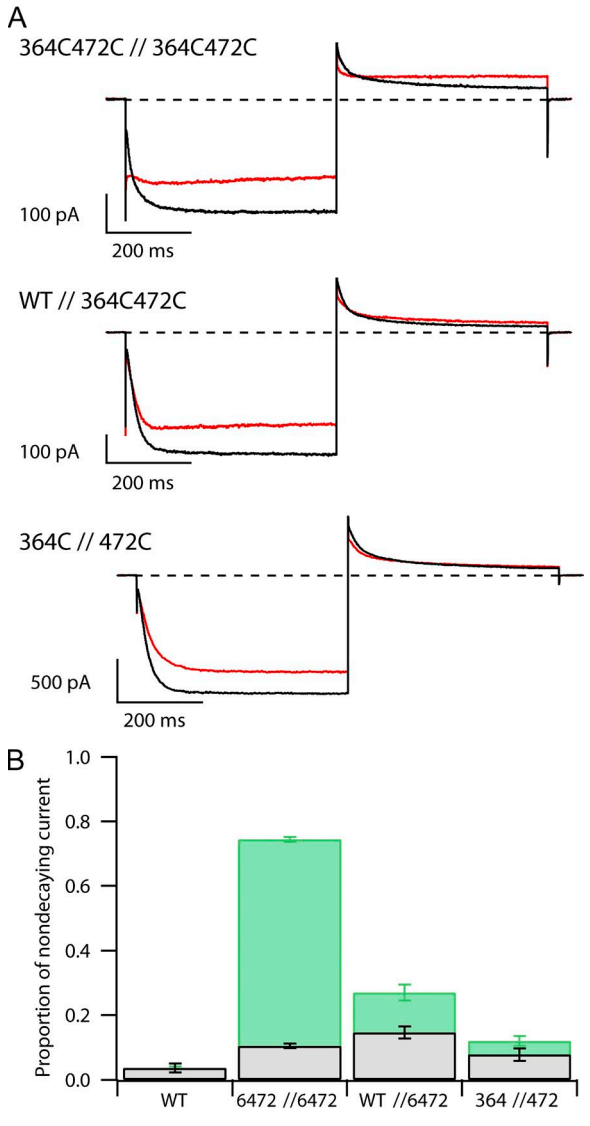

Figure 5. Use of concatenated subunits shows that in the open state metal bridges can form between A364C and S472C, possibly within the same subunit. (A) Representative current traces were recorded in the absence (black) or presence (red) of 1 μM Cd^{2+} from inside-out patches expressing one of the tandem dimers (364C472C_364C472C, WT_364C472C, or 364C_472C). Currents were elicited by 500-ms voltage steps to −120 mV from a holding potential of 0 mV, followed by a voltage step to +50 mV. (B) Effects of Cd^{2+} on the average proportions of nondecaying tail current produced by the three tandem–dimeric constructs.

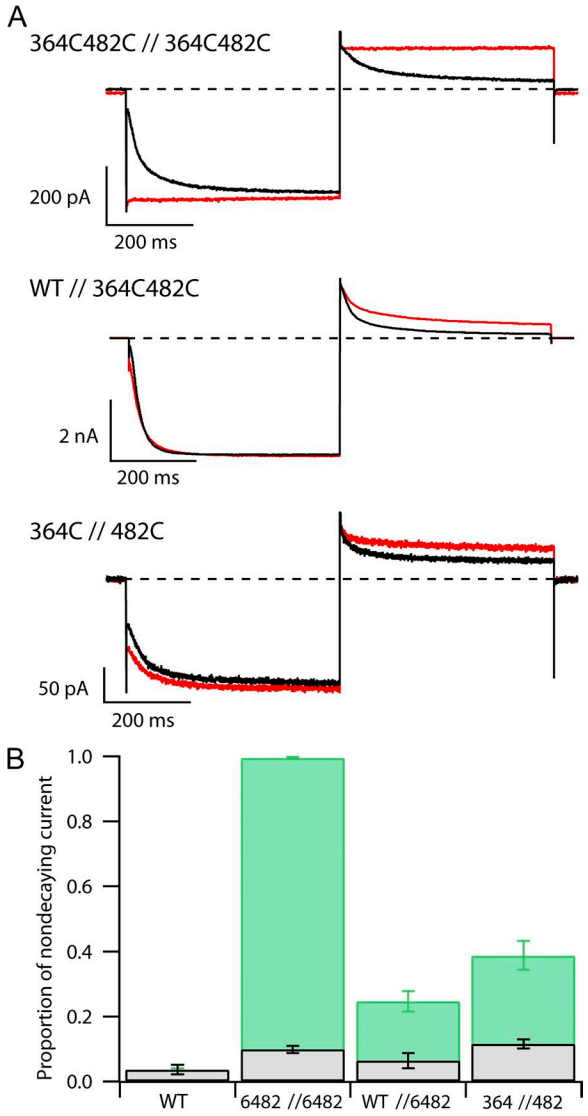

Figure 6. Intersubunit metal bridges can form between A364C and E482C in the open state. (A) Representative current traces were recorded in the absence (black) or presence (red) of 1 μM Cd^{2+} from excised inside-out patches expressing one of the tandem dimers (364C482C_364C482C, WT_364C482C, or 364C_482C). Currents were elicited by 500-ms voltage steps to −120 mV from a holding potential of 0 mV, followed by a voltage step to +50 mV. (B) Effects of Cd^{2+} on the average proportions of nondecaying tail currents produced by the three tandem dimers.

introduced cysteines in the intersubunit dimers. It remains possible that additional intrasubunit interactions also exist.

DISCUSSION

Interactions between the S4–S5 linker and lower S6/C-linker in electromechanical coupling

The S4–S5 linker of both Kv channels and HCN channels is a key component in coupling movement of the S4 voltage sensor to opening of the pore (McCormack et al., 1991; Chen et al., 2001; Long et al., 2005b). A functional interaction between the S4–S5 linker and lower S6 has been demonstrated in both Kv channels (Lu et al., 2002; Tristani-Firouzi et al., 2002; Ferrer et al., 2006) and HCN channels (Chen et al., 2001; Decher et al., 2004; Prole and Yellen, 2006). It has also been shown that a "compatible" S4–S5 linker is required in Kv channels to open the activation gate in S6 (Lu et al., 2002). In this study, the conformation of the S4–S5 linker with respect to the lower S6/C-linker in both open and closed states of cAMP-bound spHCN channels was investigated using double cysteine mutants combined with a Cd^{2+} scan. This method has previously been used effectively for determining structure–function relationships in channels (Yellen et al., 1994; Liu et al., 1997).

The ability of Cd^{2+} to produce high affinity effects on double cysteine mutant channels indicates that the sulfhydryl groups of the introduced cysteines can approach each other closely, within ~5 Å (Naylor et al., 1998; Jalilehvand et al., 2009a,b, 2011; Mah and Jalilehvand, 2010). This does not necessarily indicate that the "normal" apposition of these sulfhydryl groups is so close, as their proximity may occur in a rare conformation that is visited only occasionally in the normal conformational ensemble. However, the ability of Cd^{2+} bridges to produce strong effects on opening or closing with a high apparent affinity indicates that there cannot be a large energetic penalty for bringing the sulfhydryl groups close enough to form a bridge; if there were, the apparent affinity would be much lower.

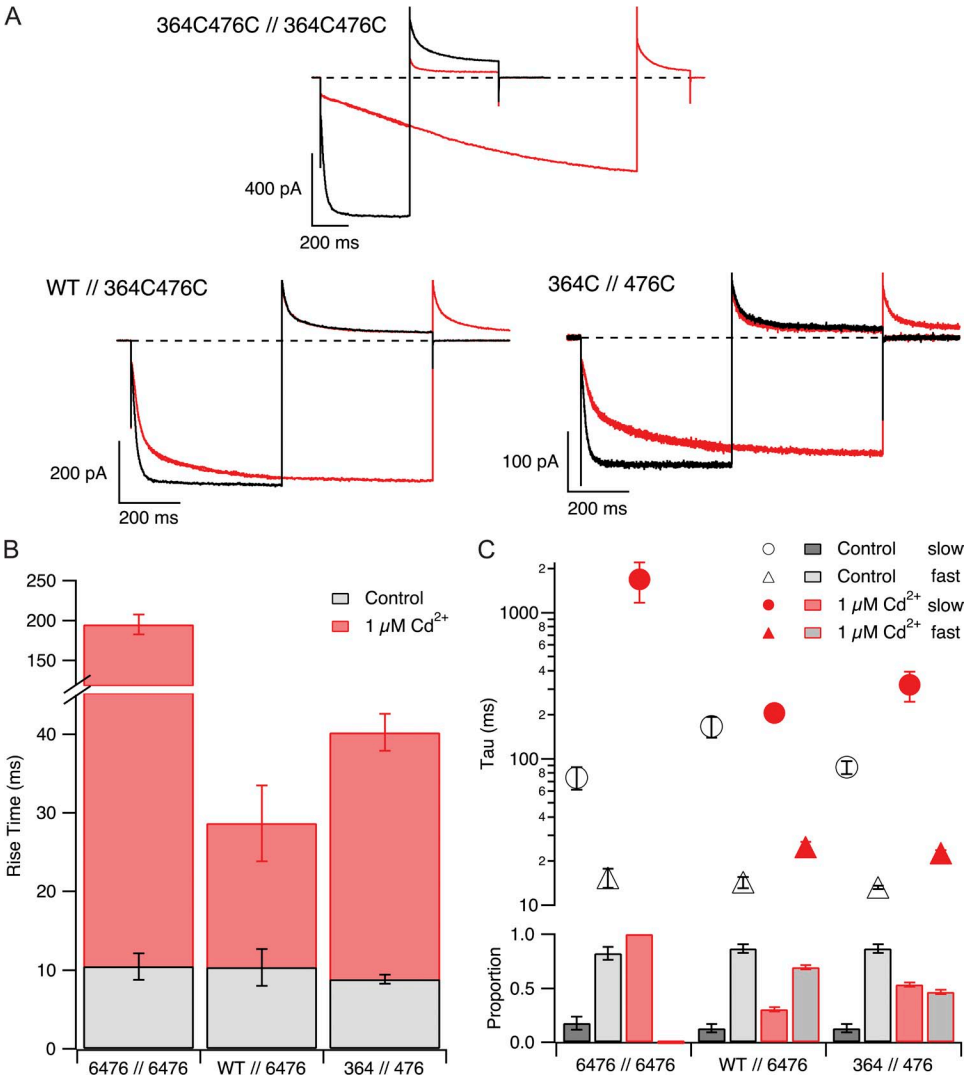

Figure 7. Intersubunit metal bridges can form between A364C and Q476C in the closed state. (A) Representative current traces were recorded in the absence (black) or presence (red) of 1 µM Cd^{2+} from excised inside-out patches expressing one of the tandem dimers (364C476C_364C476C, WT_364C476C, or 364C_476C). Currents were elicited by voltage steps to −120 mV from a holding potential of 0 mV, followed by a voltage step to +50 mV. Currents from a 2-s (364C476C_364C476C) or 1-s (WT_364C476C and 364C_476C) hyperpolarizing pulse in the presence of Cd^{2+} are superimposed on the control current traces to highlight the slowing of the activation kinetics by Cd^{2+}. (B) Effects of Cd^{2+} on the average rise time of currents produced by the intersubunit (364C_476C) and intrasubunit (WT_364C476C) tandem dimers. (C) The time course of activation was fit to a double-exponential function, and the time constants for the two components, along with the relative proportion of the slow component, are shown. The slowing of activation kinetics was mainly caused by an increase in the proportion of the slow time constant (tau).

We can estimate the expected affinity of an unstrained Cd^{2+} bridge between two cysteines by comparing the known affinities of metal binding sites. For a single cysteine ligand, weak Cd^{2+} binding affinities on the order of $10^{-3.8}$ M are commonly observed (e.g., Heinemann et al., 1992; Puljung and Zagotta, 2011). For a well-ordered zinc finger peptide with four cysteines, the Cd^{2+}-binding affinity is $\sim 10^{-13.4}$ M (Krizek et al., 1993). The difference implies roughly 3.2 orders of magnitude for each additional well-placed cysteine ligand after the first, i.e., $\sim 10^{-7}$ M (100 nM) for two cysteine ligands. This approximate affinity is in the right ballpark to explain the ability of ~130 nM of free Cd^{2+} to stabilize the open or closed states in the face of voltage stimuli that should disfavor these states. Thus, it seems that the lock-open and lock-closed effects observed here are unlikely to involve cysteine appositions requiring a substantial conformational strain compared with the native open and closed states.

Metal bridges formed between cysteines in the S4–S5 linker and lower S6/C-linker result in the trapping of spHCN channels in either the open or closed state, depending on the location of the cysteine pairs. This suggests that these regions move relative to each other during gating. In the open state, residues 359, 361, and 364 in the S4–S5 linker move into close proximity to two distinct regions in the C-linker, centered around residues 472 and 485 (Fig. 4). Residue 364 moves close to residue 476, which is sandwiched between these two regions, when the channel closes (Fig. 4). These results led us to hypothesize that the S4–S5 linker of a given subunit is involved in interactions with the C-linkers from two different subunits. The use of tandem dimers revealed that 364C can interact with 476C (in the closed state) and 482C (in the open state) from a neighboring subunit. To our knowledge, this is the first direct evidence that an intersubunit interaction can occur between the S4–S5 linker and post-S6/C-linker regions of HCN channels. Our results do not rule out the existence of additional intrasubunit interactions, as the dimers are incapable of conclusively addressing this possibility.

Comparisons with crystal structures of Kv channels

One of the most prominent features in the crystal structure of Kv1.2 is that the S4–S5 linker of a particular subunit sits on top of the S6 from the same subunit in the open state (Long et al., 2005a,b). A "downward" motion of the S4–S5 linker pushing on the lower S6 of the same subunit (i.e., intrasubunit interaction) has been hypothesized to close the activation gate, with the S4–S5 linker and lower S6 remaining attached to each other throughout the gating process (Long et al., 2005b). This model has not yet been subjected to experimental validation, and the closed conformation of Kv channels has remained elusive.

The metal bridges that we observed in this study are difficult to map onto the crystal structures of Kv channels (Long et al., 2005b, 2007; Chen et al., 2010). For example, the distances between β carbons of Kv1.2-A323 and Kv1.2-E420 (homologous to spHCN-F364 and spHCN-S474, which can be bridged by Cd^{2+} in the closed state) are too great for Cd^{2+} bridges to form: >14 Å within the same subunit and >19 Å between adjacent subunits. Likewise, the distances between Kv1.2-A323 and Kv1.2-H418 (homologous to spHCN-F364 and spHCN-S472, which can be bridged by Cd^{2+} in the open state) are also too great for Cd^{2+} bridges to form: >15 Å either within the same subunit or between adjacent subunits. Hence, the crystal structures of Kv channels appear inconsistent with our functional data for spHCN channels. This suggests that HCN channels have a different structure and gating mechanism, which may underlie their unique voltage dependence.

Spatial mapping of metal bridges defines a structural model of HCN channel gating

In choosing a starting model for the structure of spHCN channels, we note that in the closed state the spHCN channel is likely to have a straight S6 bundle similar to that of the KcsA channel (Rothberg et al., 2002, 2003). In addition, from our data we conclude that in spHCN channels bound to cAMP, the A′ helices are likely to be roughly parallel with the membrane, consistent with crystal structures of the cAMP-bound CNBD (Zagotta et al., 2003; Flynn et al., 2007). Our data are not consistent with a perpendicular (upright) disposition of the A′ helices with respect to the membrane, as proposed for the open state of CNG channels (Hua and Gordon, 2005). Such an arrangement would likely preclude the close apposition of the S4–S5 linkers and A′ helices needed to form metal bridges, in both the closed and open states. Even if an unanticipated position of S4–S5 were to make one of these interactions (364C-472C and 364C-485C) possible, the vertical disposition of the C-linker proposed by Hua and Gordon (2005) would likely rule out the interaction of 364C in the open state with both 472C and 485C, as seen here. We therefore used crystal structures of the KcsA channel and the cAMP-bound CNBD of spHCN channels in our starting model of the cAMP-bound closed state. These crystal structures were docked in a manner that allowed continuity of the lower S6 of KcsA and the A′ helix of the C-linker in spHCN (Fig. 8 A). Interestingly, this necessitates a sharp bend at the lower S6/C-linker boundary, in the vicinity of a series of three serine residues (Fig. 8 A). Consistent with this location of a bend, serine residues have only weak helical propensity, as well as a tendency to form kinks in α helices via hydrogen bonding to upstream carbonyl groups (Ballesteros et al., 2000; Deupi et al., 2010).

The locations of lock-open and lock-closed bridges for each S4–S5 linker residue examined were then mapped onto the CNBD structure (shown for 364C in

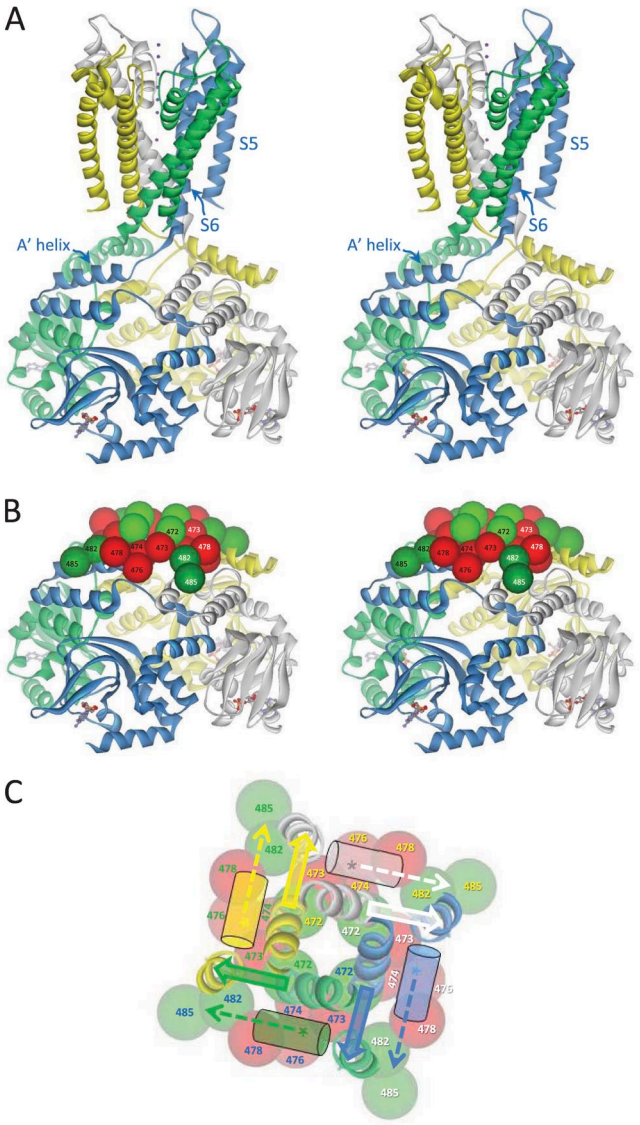

Figure 8. Model of the structure and gating motions of an HCN channel based on high affinity metal bridges. (A) Stereo view of a model of the cAMP-bound closed state of the spHCN channel, based on the crystal structures of KcsA (Protein Data Bank accession no. 1K4C) and the cAMP-bound CNBD of spHCN (Protein Data Bank accession no. 2PTM). Residue D471 of spHCN is in approximately the same position as KcsA-118, based on the equivalence of spHCN-468 to KcsA-115 (Rothberg et al., 2003). The uncoiled strands between the S6 helices and the A′ helices include the spHCN residues ^{472}SSS^{474}. (B) Stereo view of the locations of C-linker residues that when mutated to cysteine form metal bridges with 364C to produce lock-open (green spheres) and lock-closed (red spheres) effects. Spheres of ~6-Å diameter are centered around the β carbon of each C-linker residue involved in bridges with 364C. (C) Model of possible motions occurring during HCN channel gating. A view from the extracellular side of the channel, showing the locations of lock-open (green) and lock-closed (red) effects with 364C, superimposed on the closed-state model. Cylinders represent each S4–S5 linker, and asterisks indicate the positions of 364C residues. The proposed motions of 364C residues (dashed arrows) and the lower ends of the S6 helices (solid arrows) during channel opening are indicated. The color of the numbers for the C-linker residues studied matches the ribbon color for the corresponding subunit.

Fig. 8 B) and introduced into the model containing the pore region (shown for 364C in Fig. 8 C). Residue 364C is predicted to lie near the lower end of S5. Consistent with the formation of metal bridges in the intersubunit dimers, lock-closed effects involving residue 364C are positioned at the bottom of each S5 helix in the model and involve residues in the A′ helix of a neighboring subunit (Fig. 8, A–C). The model rationalizes the observation that in the open state, cysteine residues in the S4–S5 linker can form metal bridges with both 472C and 482C/485C, as in the model these C-linker residues from adjacent subunits are relatively close together at the corners of the CNBD (Fig. 8, A–C). This suggests that the proximity of the N- and C-terminal ends of A′ helices in neighboring subunits is preserved in the open state and that the A′ helices remain roughly parallel with the membrane, despite the presence of salt bridges in the CNBD that specifically stabilize the closed state (Craven and Zagotta, 2004). Interestingly, some of the cysteines involved in forming metal bridges between the S4–S5 linkers and C-linkers are located on opposite sides of putative α helices, suggesting a degree of rotational flexibility in both these regions during gating.

The spatially separated positions of lock-closed and lock-open bridges involving 364C (Fig. 8 C) suggest a substantial movement of the lower end of S5 relative to the C-linker during channel opening. The ability of 364C to form lock-open bridges with both 472C (possibly from the same subunit) and 482C/485C (likely from an adjacent subunit) suggests that these C-linker residues are both within 5 Å of 364C in the open state. The spatial separation of lock-open effects involving 472C and 482C/485C in our closed-state model (Fig. 8, B and C) suggests that these residues must move closer together during channel opening. Although other models are possible, when taken together, our data are consistent with a movement of the lower end of S5 around the central axis of the channel (Fig. 8 C, dashed arrows) causing a tilting of the S6 helices (Fig. 8 C, solid arrows), widening the intracellular entrance to the pore and causing the channel to open. These movements would bring both 364C and 472C from the same subunit close to 482C/485C from an adjacent subunit. Rotation of the C-linkers in response to movement of S6 may also occur (Craven et al., 2008), which would alter the magnitude of S5/S6 displacements required to fit our data.

In summary, we propose that in HCN channels, the main effect of the voltage sensors is to move the lower end of each S5 helix around the central axis of the channel, permitting outward movement and tilting of the S6 helices, which opens the channel. The proposed centrifugal or twisting movement of S5 on hyperpolarization contrasts with some mechanisms proposed for Kv channels, where the lower S5 is relatively static and the S4–S5 linkers mainly push down on the lower S6

regions to cause channel closure (Long et al., 2005b, 2007). The hypothesized difference between closed states—the bent S6 of Kv channels (Webster et al., 2004; Pathak et al., 2007) versus the straight S6 of HCN channels (Rothberg et al., 2003)—may largely prevent direct contact between the S4–S5 linker and S6 in HCN channels and make movement of S5 the primary sensor-to-gate interaction. One suggested mechanism for Kv channel gating includes both points of interaction (pulling on the S5 as well as the S4–S5 linker to S6 contact; Pathak et al., 2007). Whether similar or different motions of the S4–S5 linker and lower S5 occur during HCN channel activation and Kv channel deactivation is therefore presently unclear. A close apposition of the S4–S5 linkers and the C-linkers may allow the CNBDs, via the C-linkers, to exert cAMP-dependent effects on the proposed movements of the S4–S5 linkers and lower S5 helices, and hence to modulate channel gating.

We thank the members of the Yellen laboratory for their advice and suggestions, and Tatiana Abramson for expert technical support.

This work was supported by a research grant from the National Institutes of Health-National Heart, Lung, and Blood Institute (R01 HL070320 to G. Yellen). D.L. Prole was funded by a Meres senior research associateship from St. John's College, Cambridge, UK.

Sharona E. Gordon served as editor.

Submitted: 31 May 2012
Accepted: 6 August 2012

REFERENCES

Ballesteros, J.A., X. Deupi, M. Olivella, E.E. Haaksma, and L. Pardo. 2000. Serine and threonine residues bend α-helices in the $\chi_1 = g^-$ conformation. *Biophys. J.* 79:2754–2760. http://dx.doi.org/10.1016/S0006-3495(00)76514-3

Bell, D.C., H.K. Turbendian, M.T. Valley, L. Zhou, J.H. Riley, S.A. Siegelbaum, and G.R. Tibbs. 2009. Probing S4 and S5 segment proximity in mammalian hyperpolarization-activated HCN channels by disulfide bridging and Cd^{2+} coordination. *Pflugers Arch.* 458:259–272. http://dx.doi.org/10.1007/s00424-008-0613-3

Chen, J., J.S. Mitcheson, M. Tristani-Firouzi, M. Lin, and M.C. Sanguinetti. 2001. The S4-S5 linker couples voltage sensing and activation of pacemaker channels. *Proc. Natl. Acad. Sci. USA.* 98:11277–11282. http://dx.doi.org/10.1073/pnas.201250598

Chen, X., Q. Wang, F. Ni, and J. Ma. 2010. Structure of the full-length Shaker potassium channel Kv1.2 by normal-mode-based X-ray crystallographic refinement. *Proc. Natl. Acad. Sci. USA.* 107:11352–11357. http://dx.doi.org/10.1073/pnas.1000142107

Craven, K.B., and W.N. Zagotta. 2004. Salt bridges and gating in the COOH-terminal region of HCN2 and CNGA1 channels. *J. Gen. Physiol.* 124:663–677. http://dx.doi.org/10.1085/jgp.200409178

Craven, K.B., and W.N. Zagotta. 2006. CNG and HCN channels: two peas, one pod. *Annu. Rev. Physiol.* 68:375–401. http://dx.doi.org/10.1146/annurev.physiol.68.040104.134728

Craven, K.B., N.B. Olivier, and W.N. Zagotta. 2008. C-terminal movement during gating in cyclic nucleotide-modulated channels. *J. Biol. Chem.* 283:14728–14738. http://dx.doi.org/10.1074/jbc.M710463200

Decher, N., J. Chen, and M.C. Sanguinetti. 2004. Voltage-dependent gating of hyperpolarization-activated, cyclic nucleotide-gated pacemaker channels: molecular coupling between the S4-S5 and C-linkers. *J. Biol. Chem.* 279:13859–13865. http://dx.doi.org/10.1074/jbc.M313704200

Deupi, X., M. Olivella, A. Sanz, N. Dölker, M. Campillo, and L. Pardo. 2010. Influence of the *g*- conformation of Ser and Thr on the structure of transmembrane helices. *J. Struct. Biol.* 169:116–123. http://dx.doi.org/10.1016/j.jsb.2009.09.009

Ferrer, T., J. Rupp, D.R. Piper, and M. Tristani-Firouzi. 2006. The S4-S5 linker directly couples voltage sensor movement to the activation gate in the human ether-a'-go-go-related gene (hERG) K^+ channel. *J. Biol. Chem.* 281:12858–12864. http://dx.doi.org/10.1074/jbc.M513518200

Flynn, G.E., K.D. Black, L.D. Islas, B. Sankaran, and W.N. Zagotta. 2007. Structure and rearrangements in the carboxy-terminal region of SpIH channels. *Structure.* 15:671–682. http://dx.doi.org/10.1016/j.str.2007.04.008

Gauss, R., R. Seifert, and U.B. Kaupp. 1998. Molecular identification of a hyperpolarization-activated channel in sea urchin sperm. *Nature.* 393:583–587. http://dx.doi.org/10.1038/31248

Heinemann, S.H., H. Terlau, and K. Imoto. 1992. Molecular basis for pharmacological differences between brain and cardiac sodium channels. *Pflugers Arch.* 422:90–92. http://dx.doi.org/10.1007/BF00381519

Hille, B. 2001. Ion Channels of Excitable Membrane. Third edition. Sinauer Associates, Inc., Sunderland, MA. 814 pp.

Holmgren, M., K.S. Shin, and G. Yellen. 1998. The activation gate of a voltage-gated K^+ channel can be trapped in the open state by an intersubunit metal bridge. *Neuron.* 21:617–621. http://dx.doi.org/10.1016/S0896-6273(00)80571-1

Hua, L., and S.E. Gordon. 2005. Functional interactions between A′ helices in the C-linker of open CNG channels. *J. Gen. Physiol.* 125:335–344. http://dx.doi.org/10.1085/jgp.200409187

Jalilehvand, F., V. Mah, B.O. Leung, J. Mink, G.M. Bernard, and L. Hajba. 2009a. Cadmium(II) cysteine complexes in the solid state: a multispectroscopic study. *Inorg. Chem.* 48:4219–4230. http://dx.doi.org/10.1021/ic900145n

Jalilehvand, F., B.O. Leung, and V. Mah. 2009b. Cadmium(II) complex formation with cysteine and penicillamine. *Inorg. Chem.* 48:5758–5771. http://dx.doi.org/10.1021/ic802278r

Jalilehvand, F., Z. Amini, K. Parmar, and E.Y. Kang. 2011. Cadmium(II) N-acetylcysteine complex formation in aqueous solution. *Dalton Trans.* 40:12771–12778. http://dx.doi.org/10.1039/c1dt11705j

Krizek, B.A., D.L. Merkle, and J.M. Berg. 1993. Ligand variation and metal ion binding specificity in zinc finger peptides. *Inorg. Chem.* 32:937–940. http://dx.doi.org/10.1021/ic00058a030

Liu, Y.M., M. Holmgren, M.E. Jurman, and G. Yellen. 1997. Gated access to the pore of a voltage-dependent K^+ channel. *Neuron.* 19:175–184. http://dx.doi.org/10.1016/S0896-6273(00)80357-8

Long, S.B., E.B. Campbell, and R. MacKinnon. 2005a. Crystal structure of a mammalian voltage-dependent *Shaker* family K^+ channel. *Science.* 309:897–903. http://dx.doi.org/10.1126/science.1116269

Long, S.B., E.B. Campbell, and R. MacKinnon. 2005b. Voltage sensor of Kv1.2: structural basis of electromechanical coupling. *Science.* 309:903–908. http://dx.doi.org/10.1126/science.1116270

Long, S.B., X. Tao, E.B. Campbell, and R. MacKinnon. 2007. Atomic structure of a voltage-dependent K^+ channel in a lipid membrane-like environment. *Nature.* 450:376–382. http://dx.doi.org/10.1038/nature06265

Lu, Z., A.M. Klem, and Y. Ramu. 2002. Coupling between voltage sensors and activation gate in voltage-gated K^+ channels. *J. Gen. Physiol.* 120:663–676. http://dx.doi.org/10.1085/jgp.20028696

Ludwig, A., X. Zong, M. Jeglitsch, F. Hofmann, and M. Biel. 1998. A family of hyperpolarization-activated mammalian cation channels. *Nature.* 393:587–591. http://dx.doi.org/10.1038/31255

Mah, V., and F. Jalilehvand. 2010. Cadmium(II) complex formation with glutathione. *J. Biol. Inorg. Chem.* 15:441–458. http://dx.doi.org/10.1007/s00775-009-0616-3

Männikkö, R., F. Elinder, and H.P. Larsson. 2002. Voltage-sensing mechanism is conserved among ion channels gated by opposite voltages. *Nature.* 419:837–841. http://dx.doi.org/10.1038/nature01038

McCormack, K., M.A. Tanouye, L.E. Iverson, J.W. Lin, M. Ramaswami, T. McCormack, J.T. Campanelli, M.K. Mathew, and B. Rudy. 1991. A role for hydrophobic residues in the voltage-dependent gating of *Shaker* K^+ channels. *Proc. Natl. Acad. Sci. USA.* 88:2931–2935. http://dx.doi.org/10.1073/pnas.88.7.2931

Naylor, C.E., J.T. Eaton, A. Howells, N. Justin, D.S. Moss, R.W. Titball, and A.K. Basak. 1998. Structure of the key toxin in gas gangrene. *Nat. Struct. Biol.* 5:738–746. http://dx.doi.org/10.1038/1447

Pathak, M.M., V. Yarov-Yarovoy, G. Agarwal, B. Roux, P. Barth, S. Kohout, F. Tombola, and E.Y. Isacoff. 2007. Closing in on the resting state of the *Shaker* K^+ channel. *Neuron.* 56:124–140. http://dx.doi.org/10.1016/j.neuron.2007.09.023

Prole, D.L., and G. Yellen. 2006. Reversal of HCN channel voltage dependence via bridging of the S4–S5 linker and post-S6. *J. Gen. Physiol.* 128:273–282. http://dx.doi.org/10.1085/jgp.200609590

Puljung, M.C., and W.N. Zagotta. 2011. Labeling of specific cysteines in proteins using reversible metal protection. *Biophys. J.* 100:2513–2521. http://dx.doi.org/10.1016/j.bpj.2011.03.063

Rothberg, B.S., K.S. Shin, P.S. Phale, and G. Yellen. 2002. Voltage-controlled gating at the intracellular entrance to a hyperpolarization-activated cation channel. *J. Gen. Physiol.* 119:83–91. http://dx.doi.org/10.1085/jgp.119.1.83

Rothberg, B.S., K.S. Shin, and G. Yellen. 2003. Movements near the gate of a hyperpolarization-activated cation channel. *J. Gen. Physiol.* 122:501–510. http://dx.doi.org/10.1085/jgp.200308928

Santoro, B., D.T. Liu, H. Yao, D. Bartsch, E.R. Kandel, S.A. Siegelbaum, and G.R. Tibbs. 1998. Identification of a gene encoding a hyperpolarization-activated pacemaker channel of brain. *Cell.* 93:717–729. http://dx.doi.org/10.1016/S0092-8674(00)81434-8

Shin, K.S., B.S. Rothberg, and G. Yellen. 2001. Blocker state dependence and trapping in hyperpolarization-activated cation channels: evidence for an intracellular activation gate. *J. Gen. Physiol.* 117:91–101. http://dx.doi.org/10.1085/jgp.117.2.91

Tristani-Firouzi, M., J. Chen, and M.C. Sanguinetti. 2002. Interactions between S4-S5 linker and S6 transmembrane domain modulate gating of HERG K^+ channels. *J. Biol. Chem.* 277:18994–19000. http://dx.doi.org/10.1074/jbc.M200410200

Webster, S.M., D. del Camino, J.P. Dekker, and G. Yellen. 2004. Intracellular gate opening in *Shaker* K^+ channels defined by high-affinity metal bridges. *Nature.* 428:864–868. http://dx.doi.org/10.1038/nature02468

Yellen, G., D. Sodickson, T.Y. Chen, and M.E. Jurman. 1994. An engineered cysteine in the external mouth of a K^+ channel allows inactivation to be modulated by metal binding. *Biophys. J.* 66:1068–1075. http://dx.doi.org/10.1016/S0006-3495(94)80888-4

Yu, F.H., V. Yarov-Yarovoy, G.A. Gutman, and W.A. Catterall. 2005. Overview of molecular relationships in the voltage-gated ion channel superfamily. *Pharmacol. Rev.* 57:387–395. http://dx.doi.org/10.1124/pr.57.4.13

Zagotta, W.N., N.B. Olivier, K.D. Black, E.C. Young, R. Olson, and E. Gouaux. 2003. Structural basis for modulation and agonist specificity of HCN pacemaker channels. *Nature.* 425:200–205. http://dx.doi.org/10.1038/nature01922